

Excitonic Properties of Chemically Synthesized 2D Organic–Inorganic Hybrid Perovskite Nanosheets

Qi Zhang, Leiqiang Chu, Feng Zhou, Wei Ji, and Goki Eda*

2D organic–inorganic hybrid perovskites (OIHPs) represent a unique class of materials with a natural quantum-well structure and quasi-2D electronic properties. Here, a versatile direct solution-based synthesis of mono- and few-layer OIHP nanosheets and a systematic study of their electronic structure as a function of the number of monolayers by photoluminescence and absorption spectroscopy are reported. The monolayers of various OIHPs are found to exhibit high electronic quality as evidenced by high quantum yield and negligible Stokes shift. It is shown that the ground exciton peak blueshifts by ≈ 40 meV when the layer thickness reduces from bulk to monolayer. It is also shown that the exciton binding energy remains effectively unchanged for $(\text{C}_6\text{H}_5(\text{CH}_2)_2\text{NH}_3)_2\text{PbI}_4$ with the number of layers. Similar trends are observed for $(\text{C}_4\text{H}_9\text{NH}_3)_2\text{PbI}_4$ in contrast to the previous report. Further, the photoluminescence lifetime is found to decrease with the number of monolayers, indicating the dominant role of surface trap states in nonradiative recombination of the electron–hole pairs.

Organic–inorganic hybrid perovskites (OIHPs) exhibit unique anisotropic crystal structure that depends on their chemical composition.^[1] Those with a chemical formula of ABX_3 where A is an organic cation, B is a bivalent metal cation, and X is a halogen anion, exhibit cubic structure and have been intensely studied as a light absorber for solar cells in recent years.^[2–4] Precursors of OIHPs can also self-organize into a van der Waals layered structure with A_2MX_4 2D layers when the organic moieties are sufficiently large to prevent formation of 3D network of corner-sharing BX_6^{4-} octahedra.^[5,6] Such OIHPs consist of alternating layers of insulating organic moieties and semiconducting inorganic component, resembling the multiple quantum well structure. Due to the naturally occurring quantum well structure and direct band gap, 2D OIHPs

exhibit unique properties that are potentially useful for photonics applications.^[7,8] OIHPs having a chemical structure of $(\text{R-NH}_3)_2\text{PbI}_4$ where R represents a large hydrocarbon or phenethyl group have been studied extensively for their ultrafast nonlinear optical response and strong excitonic character arising from dielectric confinement effect.^[9–16]

Similar to graphene and its inorganic analogues such as transition metal dichalcogenides (TMDs),^[17–20] nanosheets (NSs) of 2D OIHPs can be isolated on a substrate by various methods and studied by optical spectroscopy. Yaffe et al.^[21] recently studied the optical properties of mechanically exfoliated 2D $(\text{C}_4\text{H}_9\text{NH}_3)_2\text{PbI}_4$ (C4PI) crystals and found that the exciton binding energy of bilayer OIHP is substantially larger than that of the corresponding layered bulk material. The reported binding energy of

490 meV for bilayer C4PI is comparable to the values for monolayer TMDs, such as WS_2 and WSe_2 , highlighting the strong excitonic nature of exfoliated C4PI at room temperature.^[22,23] This finding suggests that the electronic properties of OIHPs are strongly influenced by surrounding dielectric environment despite the insulating organic layers encapsulating each inorganic layer. The large exciton binding energy of OIHP NSs makes them an excellent candidate for the investigation of exciton-polaritons^[24] and development of novel photonic devices.^[25]

Due to the low formation energy, OIHP crystals can be synthesized in solution phase. Dou et al.^[26] recently demonstrated synthesis of ultrathin OIHP crystals with C4 alkyl chain termination using ternary solvent coevaporation technique. The process involves self-assembly and precipitation of precursors from a ternary mixture of good and poor solvents upon mild heating. The precipitation is accompanied by self-organization and formation of OIHP crystals yielding NSs with lateral sizes of a few micrometers. Following the same recipe, Chen et al. systematically investigated the controllable growth of $(\text{C}_4\text{H}_9\text{NH}_3)_2\text{PbBr}_4$.^[27] Using a similar approach, synthesis of sub-micrometer-sized $(\text{C}_6\text{H}_5(\text{CH}_2)_2\text{NH}_3)_2\text{PbI}_4$ (PEPI) NSs was recently reported by Yang et al.^[28] However, controllable synthesis of high quality ultrathin NSs that are sufficiently large for systematic microspectroscopic studies has remained a challenge.

Here, we report versatile solution-based synthesis of C4PI and PEPI NSs (see **Figure 1a** for their crystal structure) having large lateral sizes ($>10 \mu\text{m}$) from a binary cosolvent at room temperature. We show that they exhibit high emission quantum yield and negligible Stokes shift. We further demonstrate that

Q. Zhang, Dr. L. Q. Chu, F. Zhou, Prof. W. Ji, Prof. G. Eda
Physics Department
National University of Singapore
2 Science Drive 3, Singapore 117542, Singapore
E-mail: g.eda@nus.edu.sg

Dr. L. Q. Chu, Prof. G. Eda
Centre for Advanced 2D Materials and Graphene Research Centre
National University of Singapore
6 Science Drive 2, Singapore 117546, Singapore
Prof. G. Eda
Chemistry Department
National University of Singapore
3 Science Drive 3, Singapore 117543, Singapore

DOI: 10.1002/adma.201704055

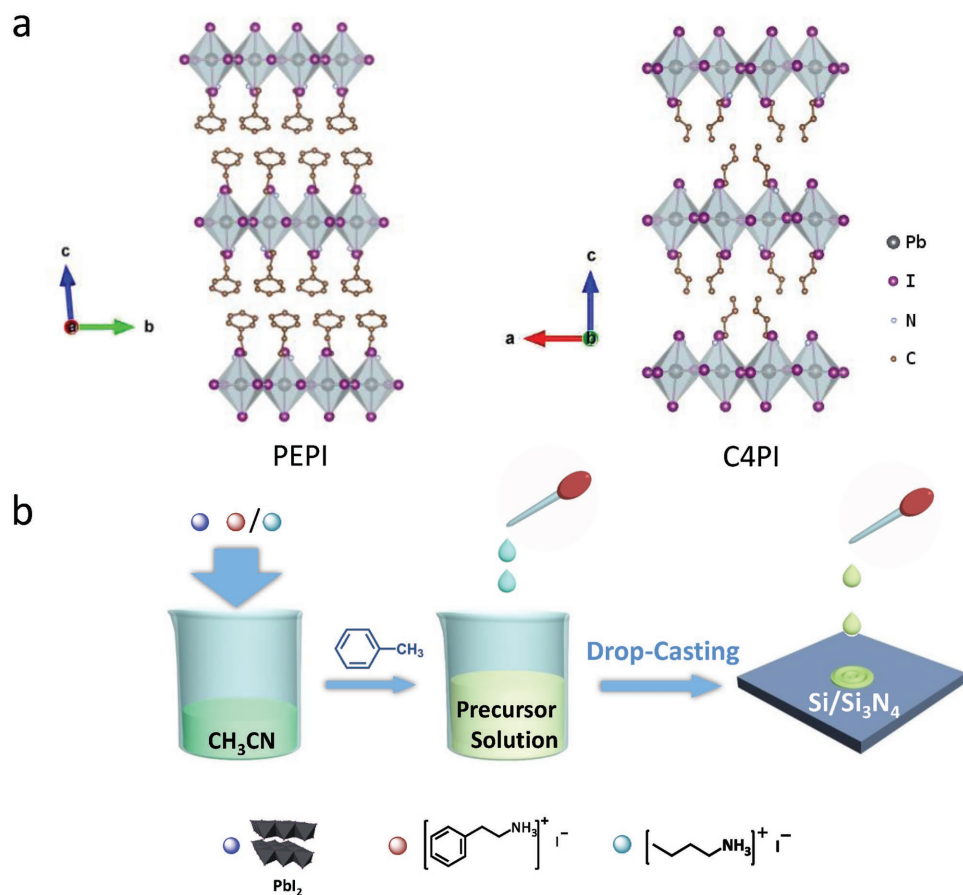


Figure 1. a) Chemical structures of PEPI and C4PI (hydrogen atoms are not shown for clarity). b) Synthesis schematics of PEPI and C4PI NSs. $\text{Si/Si}_3\text{N}_4$ substrate was selected to give high optical contrast. Substrate can also be Si/SiO_2 or fused quartz.

the optical band gap of both C4PI and PEPI scales weakly with the number of layers. Using photoluminescence spectroscopy, we reveal that the exciton binding energy and electronic band gap of PEPI are effectively independent on the number of layers in contrast to the previously reported findings on C4PI.^[21]

We used a binary mixture of good and poor solvents for the perovskite precursors instead of a ternary solvent reported previously.^[26] We tested various combinations of solvents and found that a mixture of acetonitrile and toluene yields larger and superior quality crystals with a higher yield. In particular, ternary solvents containing N,N-dimethylformamide, which was previously used for the synthesis of bromide-based 2D perovskite, yielded NSs with limited size and poor thickness homogeneity. Acetonitrile is a good solvent for the precursors while toluene is a poor solvent and induces the precipitation of the perovskite crystals. The two solvents are perfectly miscible and slowly coevaporate at room temperature, allowing controlled synthesis. Figure 1b displays the synthesis procedure. We synthesized OIHP for a range of precursor concentrations between 0.5 and 2 mg mL⁻¹ (Figures S1–S4, Supporting Information). For the synthesis of PEPI NSs, $\text{C}_6\text{H}_5(\text{CH}_2)_2\text{NH}_3\text{I}$ (PEI) and lead(II) iodide (PbI_2) powders in weight ratio of 60:40 were dissolved in acetonitrile to achieve a precursor solution of a desired concentration (see Experimental Section for the synthesis of PEI and C4I). Then toluene was added slowly into

this precursor solution until the solvent volume ratio reached 1:3 (acetonitrile:toluene). A small volume of this binary solution (7 μL) was drop-cast onto a substrate and the solvent was allowed to evaporate completely under ambient condition. NSs were formed during solvent evaporation and deposited on the substrate. Similar procedures were followed for the synthesis of C4PI. The weight ratio of the ammonium salt and PbI_2 was varied to optimize the morphology of the final product (Figures S1–S4, Supporting Information).

After complete evaporation of the solvents, micrometer-sized flakes with distinct shapes and various thicknesses were found across the substrate as shown in Figure 2a–d. The flakes exhibited photoluminescence (PL) peaked at around 516–528 nm (will be discussed in next section), which is characteristic band gap excitonic emission of PEPI and C4PI.^[29] Figure 2a–d shows changes in flake morphologies for two different precursor concentrations, namely 0.5 mg mL⁻¹ (2a and 2c) and 2 mg mL⁻¹ (2b and 2d), revealing its effect on the average flake thickness. It is worth noting that monolayer flakes of both C4PI and PEPI were obtained with nearly identical synthesis parameters. The thickness and lateral size distributions of C4PI and PEPI lakes are shown in Figure S5 (Supporting Information). We found this synthesis protocol can be applied to other 2D OIHPs having similar chemistry. Figure 2e–g shows the bright field images of ultrathin C6PI, C12PI, and

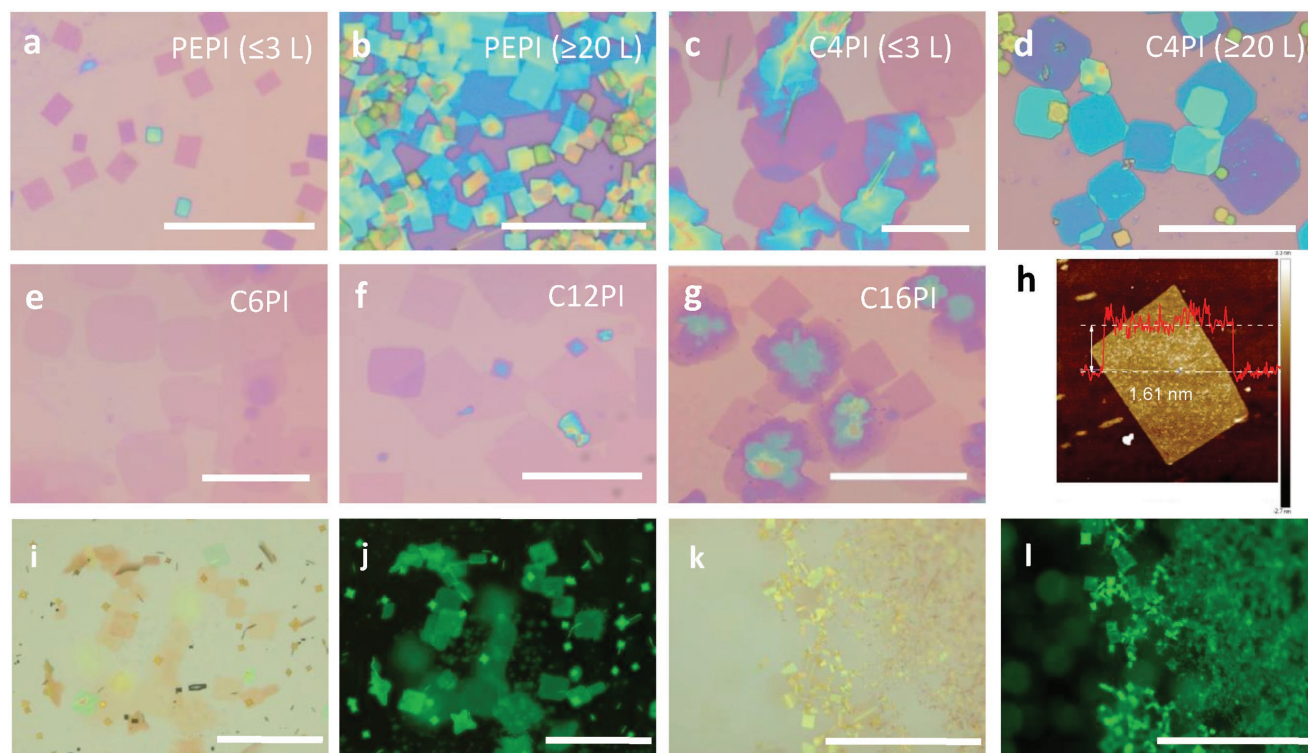


Figure 2. Optical images of a) thin PEPI NSs, b) thick PEPI NSs, c) thin C4PI NSs, d) thick C4PI NSs. e–g) Optical images of C6PI, C12PI, and C16PI thin NSs. h) AFM image and height profile of monolayer PEPI. i) Bright field and j) PL images of C4PI NSs suspending in precursor solution. k) Bright field and l) PL images of PEPI NSs suspending in precursor solution. Scale bars for (a)–(g) are 20 μm , for (i)–(l) are 50 μm .

C16PI NSs, respectively. We verified their crystal structure and high crystallinity by X-ray diffraction (XRD) measurement (Figure S6, Supporting Information). Most flakes were either rectangular or square in shape, occasionally with truncated edges, reflecting the orthorhombic crystal structure of these materials. Atomic force microscopy (AFM) analysis reveals that the thinnest flakes show a step height of ≈ 1.6 nm, which corresponds to the thickness of a monolayer PEPI (Figure 2h; Figure S7, Supporting Information).^[30] AFM images of thicker flakes are presented in the Supporting Information (Figures S8 and S9, Supporting Information). Thick flakes (>30 nm) were typically more stable in ambient conditions than mono- to few-layer flakes which tended to degrade over several minutes to hours as evidenced by reduction in PL intensity and changes in surface morphology most likely due to dissociation of organic ligands (Figure S10, Supporting Information). PEPI flakes exhibited superior stability over C4PI probably due to their highly hydrophobic organic moieties.

As-deposited flakes of different orientations were overlapped in a random manner, suggesting that nucleation occurred in the solution phase and deposition took place after complete growth of these crystallites. In order to verify this, we monitored the nucleation and growth of the crystals in situ in liquid under optical microscope. Figures 2i–l show the bright field and fluorescence microscopy images of C4PI and PEPI flakes in liquid phase during precipitation of crystal. The flakes with distinct shape with characteristic PL can be clearly seen, further evidencing liquid phase growth of these crystals. In the following discussions, thin and thick flakes refer to crystals containing

less than three monolayers (≤ 3 L) and those consisting of more than 20 monolayers (≥ 20 L), respectively.

We investigated the electronic properties of C4PI and PEPI flakes having different thicknesses using differential reflectance (DR) and PL spectroscopy. For a thin sample on a transparent substrate, DR is proportional to the absorption coefficient of the sample and can be used to obtain its approximate absorption spectrum.^[31] All optical measurements were performed in vacuum except transmittance measurements which were conducted in ambient condition.

Figure 3a shows the normalized DR and PL spectra of a thin (≤ 3 L) and thick (≥ 20 L) PEPI flakes measured at room temperature. The spectra are nearly identical for the two samples and are dominated by the characteristic ground (1s) exciton feature. The Stokes shift, which is the energy difference between excitonic peak in DR and PL, is negligible (<10 meV), indicating the high quality of PEPI samples. Figure 3b shows that C4PI flakes exhibit similar ground exciton features in the DR and PL spectra. In contrast to PEPI, the Stokes shift is more evident (≈ 11 meV) for both thin and thick C4PI samples. Further, the asymmetric PL peak of C4PI suggests that multiple emission species such as defect-bound excitons are responsible for the emission,^[10,29] while PEPI flakes typically exhibit comparatively sharper (full width at half maximum (FWHM) ≈ 59 meV) and more symmetric emission peak. Figure 3c shows reflectance, transmittance, and absorption spectra of a thick PEPI and C4PI flakes measured at room temperature. Both samples exhibit strong excitonic absorption ($\approx 55\%$) with an extracted absorption coefficient of $\approx 1.87 \times 10^5 \text{ cm}^{-1}$ at the ground exciton resonance

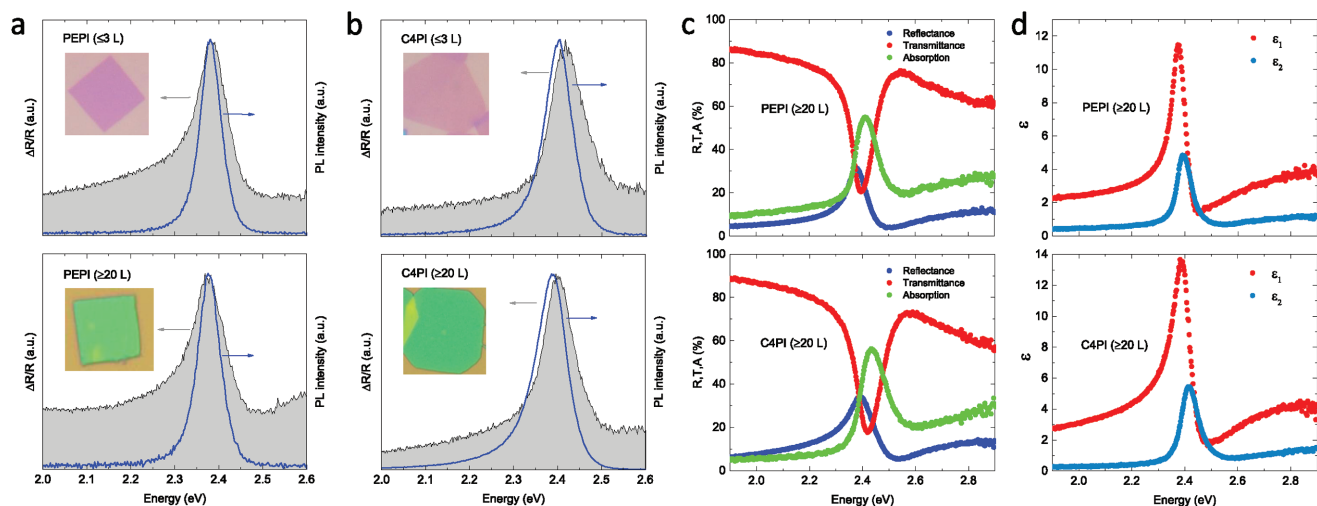


Figure 3. DR and PL spectra of: a) PEPI and b) C4PI for thin and thick NSs, respectively. Insets show optical images of corresponding perovskite flakes. c) Reflectance, transmittance, and absorption spectra of thick PEPI and C4PI NSs. d) Dielectric functions of thick PEPI and C4PI NSs.

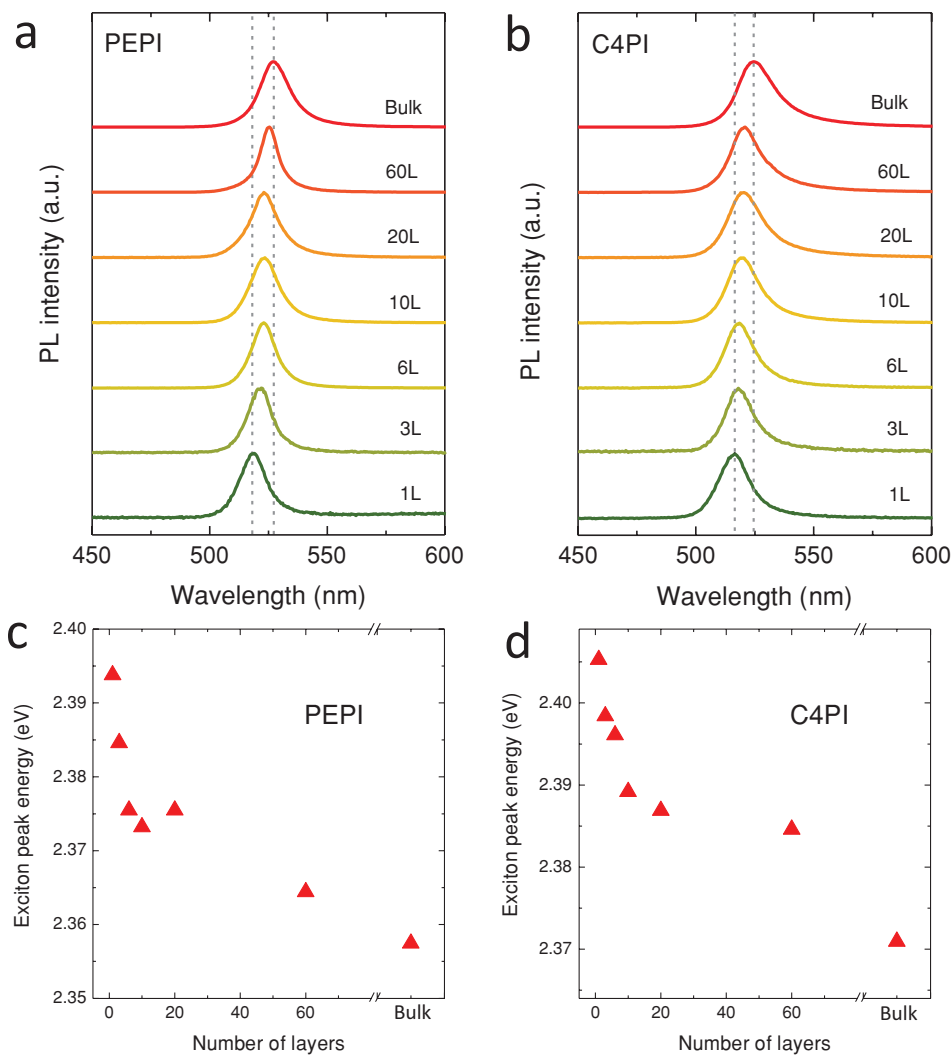


Figure 4. Thickness-dependent PL spectra of: a) PEPI and b) C4PI NSs. The dashed lines are guides for the eye. Optical band gap of: c) PEPI and d) C4PI NSs as a function of layer numbers.

(see Supporting Information for calculation method), which is in accordance with the previously reported values.^[10,21] Similar absorption values of the PEPI and C4PI samples suggest that organic moiety plays a minor role in the ground exciton absorption.^[32] From the reflectance and transmittance spectra, we obtained the dielectric function of these two samples as shown in Figure 3d. The high-frequency dielectric constant of both samples is ≈ 4.0 in agreement with the reported values for the bulk materials.^[10]

Figure 4a,b displays the normalized PL spectra of PEPI and C4PI flakes with different thicknesses. It can be seen that the optical gap is weakly dependent on the thickness of the flakes and the emission peak energy difference between monolayer and bulk samples is about 35 meV for both materials. Figure 4c,d shows that this thickness dependent shift is prominent for thicknesses below ≈ 20 monolayers. We conducted PL measurements of PEPI and C4PI flakes on various substrates with different dielectric constants but did not observe significant peak shift suggesting that substrate dielectric screening^[33] plays a minor role (Figure S11, Supporting Information). Similar thickness-dependent trends were observed for C6PI, C12PI, and C16PI as shown in Figure S12 (Supporting Information).

Ground exciton peak energy is determined by quasiparticle band gap and exciton binding energy. It has been shown that both these quantities scale with the number of layers for TMDs due to strong interlayer screening.^[34] The absence of prominent PL energy shift with flake thickness therefore does not rule out the possibility of interlayer coupling in C4PI and PEPI samples. Thus, exciton binding energy needs to be independently measured in order to understand the thickness scaling effect. Yaffe et al.^[21] extracted the exciton binding energy of mechanically exfoliated bilayer C4PI from the energy of higher order exciton peaks that appear in DR spectra at 5K. These higher order exciton peaks were not observable in our sample at

liquid nitrogen temperature. Here we use photoluminescence excitation (PLE) spectroscopy to investigate the transitions above the optical band gap.^[35]

Figure 5a shows the PL and PLE spectra of PEPI flakes with different thicknesses at 78K. In contrast to the DR spectra, the excitation spectra reveal a region of almost fully suppressed PL followed by a distinct onset of absorption around 2.56 eV. This step-like increase in absorption, which is a signature of free carrier absorption in 2D electronic systems, matches very well with the previously reported band edge absorption.^[10] Thus we conclude this energy to be the electronic gap of these materials. This electronic band gap is almost identical for thick and thin samples. These observations also indicate that exciton binding energy of PEPI remains nearly constant (≈ 200 meV) and its electronic structure depends only weakly on the flake thickness. The PLE spectra of thin and thick C4PI also show similar abrupt onset near 2.8 eV. Note that here we monitored the emission intensity of the low temperature (LT) phase peak (≈ 2.53 eV) that emerges below ≈ 250 K.^[11,21] Assuming that there is no energy transfer between different phases, we estimate the binding energy of the LT phase to be ≈ 260 meV for both thin and thick C4PI flakes. Figure 5c summarizes the exciton binding energies of PEPI and C4PI measured in this work and those reported in literature for PEPI and C4PI with different thicknesses. We believe that the discrepancies arise from the uncertainty of different estimation methods employed by different groups.

We measured room-temperature exciton lifetime of isolated individual PEPI flakes in vacuum ($\approx 10^{-5}$ mbar) using the time-correlated single photon counting technique. For both PEPI and C4PI, we found the exciton average lifetime to decrease gradually with decreasing thickness of the flake as shown in Figure 6a. The decay curves were fitted with a biexponential function and fast (τ_1) and slow (τ_2) decay lifetimes were extracted. These decay times were found to be $\tau_1 = 166$ ps (16.8%) and $\tau_2 = 1037$ ps

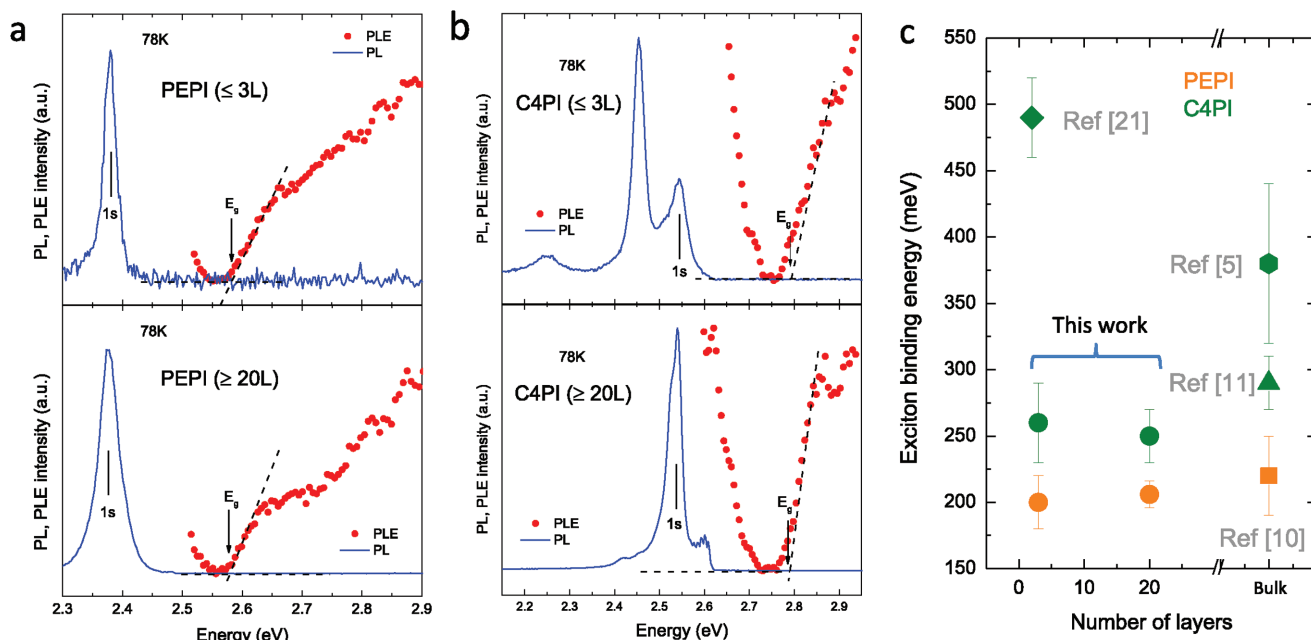


Figure 5. a) PL and PLE spectra of thin and thick PEPI NSs at 78 K. b) PL and PLE spectra of thin and thick C4PI NSs at 78 K. Band gap positions are extracted by Tauc plot and they are indicated in the plots. c) Summary of exciton binding energy for PEPI and C4PI with different thickness.

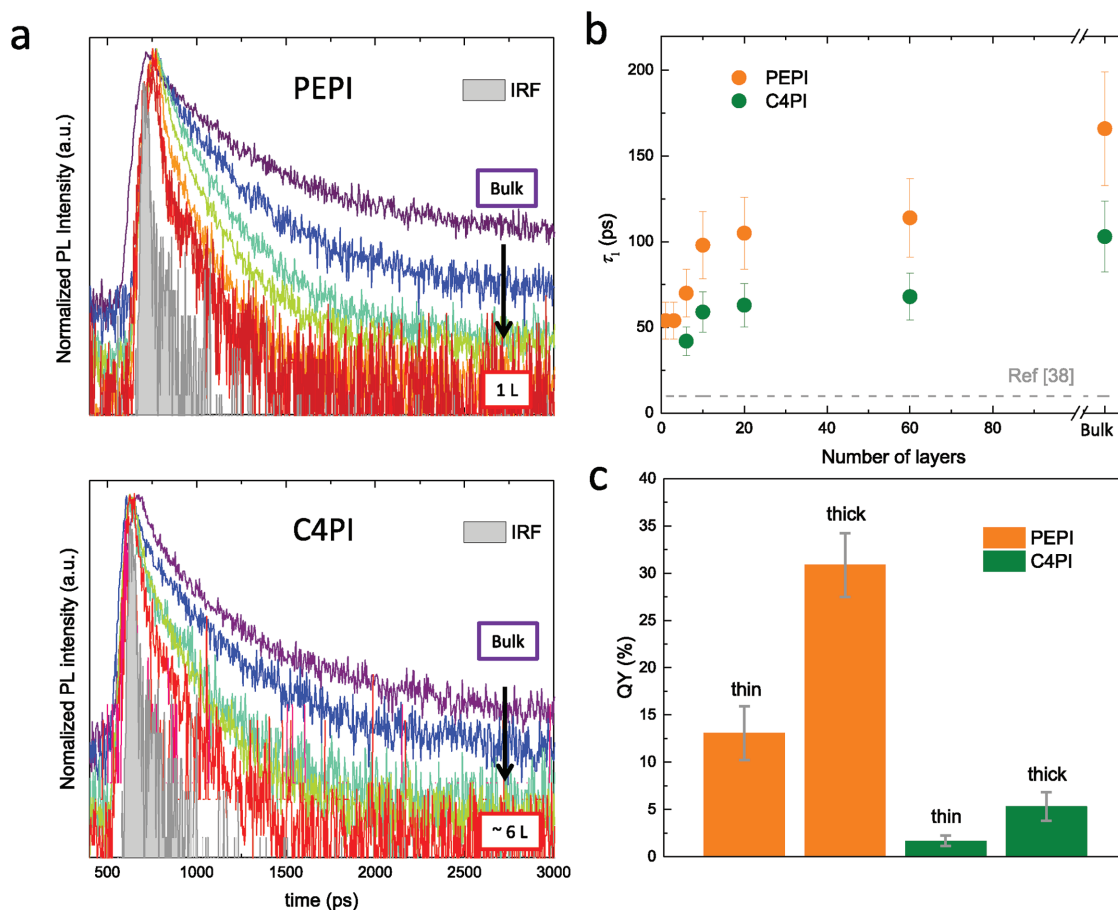


Figure 6. a) Room temperature PL decay curves of PEPI and C4PI NSs with thickness from bulk to thin. b) Evolution of fast decay time (τ_1) for PEPI and C4PI NSs as a function of layer numbers. c) QY of PEPI and C4PI NSs with different thickness.

(83.2%) for the bulk PEPI crystal and $\tau_1 = 103$ ps (36.0%) and $\tau_2 = 530$ ps (64.0%) for the bulk C4PI crystal (see Table S1 in the Supporting Information). These decay times are comparable to the lifetimes reported for PEPB and C4PI crystals that are considered to be of high quality due to slow precipitation growth.^[36,37] On the other hand, they are an order of magnitude longer compared to the lifetimes reported for polycrystalline PEPI thin film samples prepared by spin-coating.^[38] The PL lifetimes were consistently lower for flakes with smaller thicknesses as summarized in Figure 6b. Furthermore, we performed thickness scaling study of intrinsic radiative rate (k_r) which can be expressed in terms of PL quantum yield (QY) and exciton lifetime (τ) as $k_r = \frac{QY}{\tau}$. We estimated the QY by measuring the integrated PL intensity of the samples relative to that of a reference dye sample with a known QY (see Experimental Section for details). Figure 6c summarizes the QY of thick and thin PEPI and C4PI samples. The PEPI flakes exhibited significantly higher QY compared with the C4PI flakes under identical measurement conditions. The estimated QY for thick and thin PEPI flakes was 31% and 13%, respectively. Combined with exciton lifetimes of these PEPI samples (54 ps for ≈ 3 L and 105 ps for ≈ 20 L), k_r was found to be of the order of 1 ns^{-1} for both PEPI samples. QY of C4PI was estimated to be 5% and 2%, for thick and thin samples, respectively. The radiative rate of

C4PI was calculated to be $\approx 0.4 \text{ ns}^{-1}$ for both samples. We thus attribute the shorter lifetime and lower QY of the thin samples to higher degree of structural defects that give rise to the fast nonradiative recombination of excitons.

In summary, we have developed a facile liquid-phase synthesis for 2D OIHP NSs with thicknesses ranging from a single monolayer to tens of monolayers. The synthesis technique is highly versatile and allows preparation of NSs with a variety of organic moieties. The PEPI NSs exhibit high PL quantum yield up to 31% with exciton lifetimes comparable to that of high quality bulk samples. We found the exciton binding energy and quasiparticle band gap of PEPI to be independent on the number of layers, which is distinctly different from the recently reported case of C4PI. Our work highlights the versatility of 2D OIHP NSs synthesis and opens up avenues for exploring their fundamental excitonic properties in solid state.

Experimental Section

Chemicals and Reagents: Phenethylamine ($\geq 99\%$), butylamine ($\geq 99\%$), hexylamine (99%), dodecylamine (98%), hexadecylamine (98%), lead(II) iodide (PbI_2) (99%), hydriodic acid (HI) (57 wt%), acetonitrile (99.7%, analytical reagent (AR)), and toluene (99.99%, high-performance liquid chromatography (HPLC)) were purchased from Sigma Aldrich. All chemicals were used as received without any further purification.

Synthesis of Ammonium Salts: Synthesis of $C_6H_5(CH_2)_2NH_3I$. 10 mL ethanol and 2.52 mL phenethylamine ($C_6H_5(CH_2)_2NH_2$) were added to a beaker to form a mixture which was kept at 0 °C using an ice bath. Stoichiometric amount of HI (2.62 mL) was added to the mixture dropwise and it was stirred for 2.5 h to ensure fully reaction. Heating the solvent at 60 °C with a rotary evaporator until whitish ammonium salt powder appeared and the solvent residue evaporated completely. The ammonium salt powder was collected and washed with diethyl ether for three times. Then the powder was transferred to a vacuum oven and dried at 60 °C for 24 h for later use. Synthesis processes of C4I, C6I, C12I, and C16I are similar to PEI, except that replacing $C_6H_5(CH_2)_2NH_2$ with corresponding amines.

Synthesis of 2D OIHP Nanosheets: (I) PEPI: 12 mg PEI and 8 mg PbI_2 were dissolved in 10 mL acetonitrile to prepare 2 mg mL^{-1} stock solution. When synthesizing relatively thick (≥ 10 L) PEPI NSs, dropped 2 mL stock solution to a vial, then added toluene dropwise to the vial until the total volume reached 8 mL. 7 μL of this cosolvent was drop-casted onto a substrate and let it evaporate naturally under ambient condition. The stock solution was diluted with acetonitrile to 0.5 mg mL^{-1} for synthesizing relatively thin (≤ 6 L) PEPI NSs. 2 mL of the diluted stock solution was dropped to a vial and followed by adding 6 mL toluene. The same drop-casting process was then conducted. (II) C4PI: 10 mg C4I and 10 mg PbI_2 were dissolved in 10 mL acetonitrile and 2 mg mL^{-1} stock solution was obtained. When synthesizing relatively thick (≥ 10 L) C4PI NSs, 2 mL stock solution was put to a vial and toluene was added dropwise until the total volume reached 10 mL. The stock solution was diluted with acetonitrile to 0.5 mg mL^{-1} for synthesizing relatively thin (≤ 6 L) C4PI NSs. 2 mL of the diluted stock solution was dropped to a vial and followed by adding 6 mL toluene. Drop-casting processes for thin and thick C4PI samples are similar to the PEPI counterparts. (III) For C6PI, C12PI, and C16PI, similar processes were performed to synthesize crystalline NSs with different thickness.

AFM Measurement: Atomic force microscope (Bruker Dimension FastScan, Tapping mode) was used to measure height profile of perovskite NSs.

X-ray Diffraction Measurement: XRD studies were performed on 2D perovskite flakes and wide-angle XRD patterns were collected on Bruker D8 Focus Powder X-ray diffractometer using $Cu K\alpha$ radiation (40 kV, 40 mA) at room temperature.

Optical Measurements: Micro-PL spectra were obtained with a laser confocal microscope (NT-MDT, NTEGR Spectra) in back scattering geometry with 473 nm (continuous wave (cw)) excitation laser. The differential reflectance of individual flakes was performed with a focused white light from a quartz tungsten light source. The DR is defined as $(R_s - R_q)/R_q$, where R_s is the reflective light intensity from sample and R_q is the counterpart of quartz substrate. Incident light intensity attenuation function is described by Beer–Lambert law as $I(t) = I_0 \exp(-\alpha t)$, where $\alpha(\lambda)$ is absorption coefficient and t is penetration depth. Thus, $\alpha(\lambda)$ can be extracted from absorption spectra when sample thickness is known. PLE spectra were obtained by a monochromator and a super-continuum light as the excitation source which is coupled to a tunable laser filter in back scattering geometry. The PLE experiment was conducted in vacuum ($\approx 10^{-5}$ mbar) at liquid nitrogen temperature since the emission will become more prominent and discernable at low temperature. The excitation intensity was kept below 50 $W cm^{-2}$ in order to avoid any nonlinear effect. Exciton lifetime measurement was also performed under vacuum ($\approx 10^{-5}$ mbar) using a picosecond pulse-laser (480 nm) with the repetition rate of 6.0 MHz and the average power of $\approx 20 W cm^{-2}$. Time-correlated single photon counting (PicoHarp 300) setup was used as the detection system. To estimate the PL quantum yield of perovskite NSs, standard dye sample (5,5''-Bis(N,N-diphenylamino)-4'-dimesitylboryl-2,2':5',2'':5'',2''''-quaterthiophene) with known QY ($\approx 36\%$) was used as reference. Absorbance of thin perovskite NSs was calculated from DR spectra using $\frac{R_s(\lambda) - R_q(\lambda)}{R_q(\lambda)} = \frac{4}{n^2 - 1} A(\lambda)$, where n is substrate refractive index and here it is assumed to be wavelength independent. Absorption of thin NSs was then obtained from $1 - 10^{-A(\lambda)}$. The QY of thin NS was obtained using $\frac{I_0 A_{perov} QY_{perov} \eta_{perov}}{I_0 A_{dye} QY_{dye} \eta_{dye}} = \frac{PL_{perov}}{PL_{dye}}$, where A is absorption and η is collection efficiency of CCD spectrometer. Extinction

and reflectance spectra measurement was performed to achieve accurate absorption values.

Supporting Information

Supporting Information is available from the Wiley Online Library or from the author.

Acknowledgements

This work was supported by MOE under AcRF Tier 2 (MOE2015-T2-2-123). The authors acknowledge the support from the National Research Foundation, Prime Minister's Office, Singapore, under its NRF research fellowship (NRF-NRF2011-02) and Medium Sized Centre Program.

Conflict of Interest

The authors declare no conflict of interest.

Keywords

2D perovskite nanosheets, dielectric screening effect, photoluminescence excitation spectroscopy, thickness scaling study

Received: July 20, 2017

Revised: January 16, 2018

Published online:

- [1] B. Saparov, D. B. Mitzi, *Chem. Rev.* **2016**, *116*, 4558.
- [2] M. Liu, M. B. Johnston, H. J. Snaith, *Nature* **2013**, *501*, 395.
- [3] A. Kojima, K. Teshima, Y. Shirai, T. Miyasaka, *J. Am. Chem. Soc.* **2009**, *131*, 6050.
- [4] J. Burschka, N. Pellet, S.-J. Moon, R. Humphry-Baker, P. Gao, M. K. Nazeeruddin, M. Grätzel, *Nature* **2013**, *499*, 316.
- [5] J.-C. Blancon, H. Tsai, W. Nie, C. Stoumpos, L. Pedesseau, C. Katan, M. Kepenekian, C. M. M. Soe, K. Appavoo, M. Sfeir, *Science* **2017**, *eaa14211*.
- [6] C. C. Stoumpos, D. H. Cao, D. J. Clark, J. Young, J. M. Rondinelli, J. I. Jang, J. T. Hupp, M. G. Kanatzidis, *Chem. Mater.* **2016**, *28*, 2852.
- [7] L. N. Quan, Y. Zhao, F. P. García de Arquer, R. Sabatini, G. Walters, O. Voznyy, R. Comin, Y. Li, J. Z. Fan, H. Tan, *Nano Lett.* **2017**, *17*, 3701.
- [8] M. Yuan, L. N. Quan, R. Comin, G. Walters, R. Sabatini, O. Voznyy, S. Hoogland, Y. Zhao, E. M. Beaugard, P. Kanjanaboos, *Nat. Nanotechnol.* **2016**, *11*, 872.
- [9] A. Brehier, R. Parashkov, J. S. Lauret, E. Deleporte, *Appl. Phys. Lett.* **2006**, *89*, 171110.
- [10] X. Hong, T. Ishihara, A. V. Nurmikko, *Phys. Rev. B: Condens. Matter* **1992**, *45*, 6961.
- [11] T. Ishihara, J. Takahashi, T. Goto, *Phys. Rev. B: Condens. Matter* **1990**, *42*, 11099.
- [12] C. R. Kagan, *Science* **1999**, *286*, 945.
- [13] D. B. Mitzi, K. Chondroudis, C. R. Kagan, *IBM J. Res. Dev.* **2001**, *45*, 29.
- [14] D. B. Mitzi, C. Feild, W. Harrison, A. Guloy, *Nature* **1994**, *369*, 467.
- [15] W. Niu, L. A. Ibbotson, D. Leipold, E. Runge, G. V. Prakash, J. J. Baumberg, *Phys. Rev. B: Condens. Matter* **2015**, *91*, 161303.

- [16] C. Symonds, J. Bellessa, J. C. Plenet, A. Bréhier, R. Parashkov, J. S. Lauret, E. Deleporte, *Appl. Phys. Lett.* **2007**, *90*, 091107.
- [17] K. F. Mak, C. Lee, J. Hone, J. Shan, T. F. Heinz, *Phys. Rev. Lett.* **2010**, *105*, 136805.
- [18] Q. H. Wang, K. Kalantar-Zadeh, A. Kis, J. N. Coleman, M. S. Strano, *Nat. Nanotechnol.* **2012**, *7*, 699.
- [19] H. Ramakrishna Matte, A. Gomathi, A. K. Manna, D. J. Late, R. Datta, S. K. Pati, C. Rao, *Angew. Chem.* **2010**, *122*, 4153.
- [20] B. Radisavljevic, A. Radenovic, J. Brivio, I. V. Giacometti, A. Kis, *Nat. Nanotechnol.* **2011**, *6*, 147.
- [21] O. Yaffe, A. Chernikov, Z. M. Norman, Y. Zhong, A. Velauthapillai, A. van der Zande, J. S. Owen, T. F. Heinz, *Phys. Rev. B: Condens. Matter* **2015**, *92*, 045414.
- [22] Z. Ye, T. Cao, K. O'Brien, H. Zhu, X. Yin, Y. Wang, S. G. Louie, X. Zhang, *Nature* **2014**, *513*, 214.
- [23] K. He, N. Kumar, L. Zhao, Z. Wang, K. F. Mak, H. Zhao, J. Shan, *Phys. Rev. Lett.* **2014**, *113*, 026803.
- [24] T. Low, A. Chaves, J. D. Caldwell, A. Kumar, N. X. Fang, P. Avouris, T. F. Heinz, F. Guinea, L. Martin-Moreno, F. Koppens, *Nat. Mater.* **2016**, *16*, 182.
- [25] Z. Tan, Y. Wu, H. Hong, J. Yin, J. Zhang, L. Lin, M. Wang, X. Sun, L. Sun, Y. Huang, *J. Am. Chem. Soc.* **2016**, *138*, 16612.
- [26] L. Dou, A. B. Wong, Y. Yu, M. Lai, N. Kornienko, S. W. Eaton, A. Fu, C. G. Bischak, J. Ma, T. Ding, *Science* **2015**, *349*, 1518.
- [27] J. Chen, L. Gan, F. Zhuge, H. Li, J. Song, H. Zeng, T. Zhai, *Angew. Chem.* **2017**, *129*, 2430.
- [28] S. Yang, W. Niu, A. L. Wang, Z. Fan, B. Chen, C. Tan, Q. Lu, H. Zhang, *Angew. Chem., Int. Ed.* **2017**, *56*, 4252.
- [29] K. Gauthron, J. Lauret, L. Doyennette, G. Lanty, A. Al Choueiry, S. Zhang, A. Brehier, L. Largeau, O. Mauguin, J. Bloch, *Opt. Express* **2010**, *18*, 5912.
- [30] E. A. Muljarov, S. Tikhodeev, N. Gippius, T. Ishihara, *Phys. Rev. B: Condens. Matter* **1995**, *51*, 14370.
- [31] K. F. Mak, M. Y. Sfeir, Y. Wu, C. H. Lui, J. A. Misewich, T. F. Heinz, *Phys. Rev. Lett.* **2008**, *101*, 196405.
- [32] A. Fraccarollo, V. Cantatore, G. Boschetto, L. Marchese, M. Cossi, *J. Chem. Phys.* **2016**, *144*, 164701.
- [33] M. L. Trolle, T. G. Pedersen, V. Vénard, *Sci. Rep.* **2017**, *7*, 39844.
- [34] W. Zhao, Z. Ghorannevis, L. Chu, M. Toh, C. Kloc, P.-H. Tan, G. Eda, *ACS Nano* **2012**, *7*, 791.
- [35] H. M. Hill, A. F. Rigosi, C. Roquelet, A. Chernikov, T. C. Berkelbach, D. R. Reichman, M. S. Hybertsen, L. E. Brus, T. F. Heinz, *Nano Lett.* **2015**, *15*, 2992.
- [36] N. Kawano, M. Koshimizu, Y. Sun, N. Yahaba, Y. Fujimoto, T. Yanagida, K. Asai, *J. Phys. Chem. C* **2014**, *118*, 9101.
- [37] Z. Guo, X. Wu, T. Zhu, X. Zhu, L. Huang, *ACS Nano* **2016**, *10*, 9992.
- [38] T. Fujita, H. Nakashima, M. Hirasawa, T. Ishihara, *J. Lumin.* **2000**, *87*, 847.